Ga_2O_3 Nanoribbons−Eu_2O_3 Multisheaths Heterostructure and Energy Transfer

Lei Fu, Zhimin Liu, Yunqi Liu,* Buxing Han, Jiaqiu Wang, Pingan Hu, Lingchao Cao, and Daoben Zhu*

Center for Molecular Science, Institute of Chemistry, Chinese Academy of Sciences, Beijing 100080, People's Republic of China

Received: April 21, 2004; In Final Form: June 9, 2004

By using a simple low-temperature supercritical fluid-assisted method, single-crystalline nanoribbons coated with crystalline multisheath oxide have been successfully synthesized, with a nominally uniform coating over the entire outer surface of the nanoribbons. The methodology reported here is highly versatile. As an example, Ga_2O_3−Eu_2O_3 core−sheath coaxial nanoribbons are synthesized and show a novel energy transfer between the core and sheath at room temperature, which is observed for the first time in our study. The structures are confirmed by HRTEM, EDX, and XPS. These core−sheath coaxial heterostructures, with their various possible functionalities, represent an important new class of nanoscale building blocks for optoelectronic applications.

1. Introduction

One-dimensional heterostructures are of particular interest with respect to potential applications as unique types of nanoscale building blocks for future optoelectronic devices and systems.[1] However, only a few recent efforts have been made on heterostructures such as superlattice nanowires and core−sheath coaxial nanowires. Diverse functions have been realized by assembling two semiconducting nanowires or nanotubes into crossed junctions.[2−5] Composite nanoribbons have been obtained through an epitaxial growth on nanoribbons or nanowires (as one-dimensional nanoscale substrates) via a pulsed laser deposition or thermal evaporation.[6−7] Novel axial semiconductor nanowire heterostructures with composition modulation have been prepared from GaAs/GaP and Si/SiGe nanowires,[8−11] and it has been demonstrated that they may have highly promising applications ranging from nanobarcodes to polarized nanoscale light-emitting diodes. Si−Ge core−sheath coaxial nanowire heterostructures have been grown by modulating the composition of the reactant gases in a process of chemical vapor deposition.[12] A significant bottleneck in this field is the lack of a general approach to the synthesis of one-dimensional heterostructures based on a simple, efficient, and low-temperature route.

The unique electronic, optical, and chemical properties of the rare earth oxides make them useful in a variety of diverse applications, such as laser materials, phosphors, and catalysis.[13] The luminescence of Eu^{3+} is particularly interesting because the major emission band is centered near 612 nm (red), which is one of the three primary colors. Eu_2O_3 is one of the most important oxide phosphors and has been studied extensively.[14−16] Monoclinic gallium oxide (β-Ga_2O_3) is a wide band gap semiconductor (E_g = 4.9 eV). It exhibits conduction and luminescence properties, and thus has potential applications in optoelectronic devices including flat-panel displays, solar energy conversion devices, optical limiter for ultraviolet, and high-temperature stable gas sensors.[17−25] Here we report a novel and versatile approach to the synthesis of various composite nanoribbon structures, and the resulting nanostructures could readily have multiple functionalities in the low-temperature range. As an example, the Ga_2O_3−Eu_2O_3 core−sheath coaxial nanoribbons are synthesized and show novel energy transfer between the core and sheath at room temperature. The reason we choose Eu_2O_3 and Ga_2O_3 as an example to introduce our novel and versatile method to synthesize core−sheath coaxial heterostructures is that not only they are important luminescence materials, but also the melting points of these oxides are extremely high (such as Eu_2O_3, 2330 °C) and therefore they are difficult to synthesize by conventional methods.

In this study, we use Ga_2O_3 nanoribbons[26] as one-dimensional nanoscale substrates for coating crystalline multiwalled europium oxide sheaths. Our synthesis is based on a novel, simple, efficient, and low-temperature route. The principle of this route is the following: Ga_2O_3 nanoribbons were first suspended in ethanol solution of europium nitrate hexahydrate in a high-pressure vessel. Then CO_2 was charged to the desired pressure at a suitable temperature, resulting in a supercritical fluid (SCF) solution. Supercritical CO_2 as an antisolvent reduced the solvent strength of ethanol,[27] which made europium nitrate precipitate from the solution and coat on the exterior walls of the Ga_2O_3 nanoribbons uniformly because high supersaturation was reached in a short time and the particles were very fine. The europium nitrate decomposed to form europium oxide at an appropriate temperature. The resulting products are Eu_2O_3−Ga_2O_3 coaxial nanoribbons, the surface of Ga_2O_3 nanoribbons being directly coated with conformal europium oxide sheaths. The thickness of europium oxide sheaths was controllable by changing the concentration of the europium(III) ion.

2. Experimental Methods

In this process, bulk quantities of Ga_2O_3 nanoribbons with high purity have been grown by a convenient hydrogen-assisted thermal evaporation method.[26] The resulting nanoribbons were characterized by outer diameters of 60−150 nm and lengths of several hundreds of micrometers. In a typical coating experiment, 2 mL of 10 wt % europium(III) nitrate hexahydrate ethanol solution and 10 mg of purified Ga_2O_3 nanoribbons were loaded into a high-pressure stainless vessel with a volume of 22 mL. After ultrasonically dispersing for about 30 min, the vessel was placed in a constant water bath of 35 °C. CO_2 was then charged with a high-pressure pump up to 9.0 MPa. Then the vessel was moved to an oven with a temperature of 120 °C at which europium(III) nitrate hexahydrate was decomposed,

* Corresponding authors. Telephone: 86-10-62613253. Fax: 86-10-62559373. E-mail: liuyq@mail.iccas.ac.cn (Y.L.).

10.1021/jp048268q CCC: $27.50
Published on Web 08/06/2004

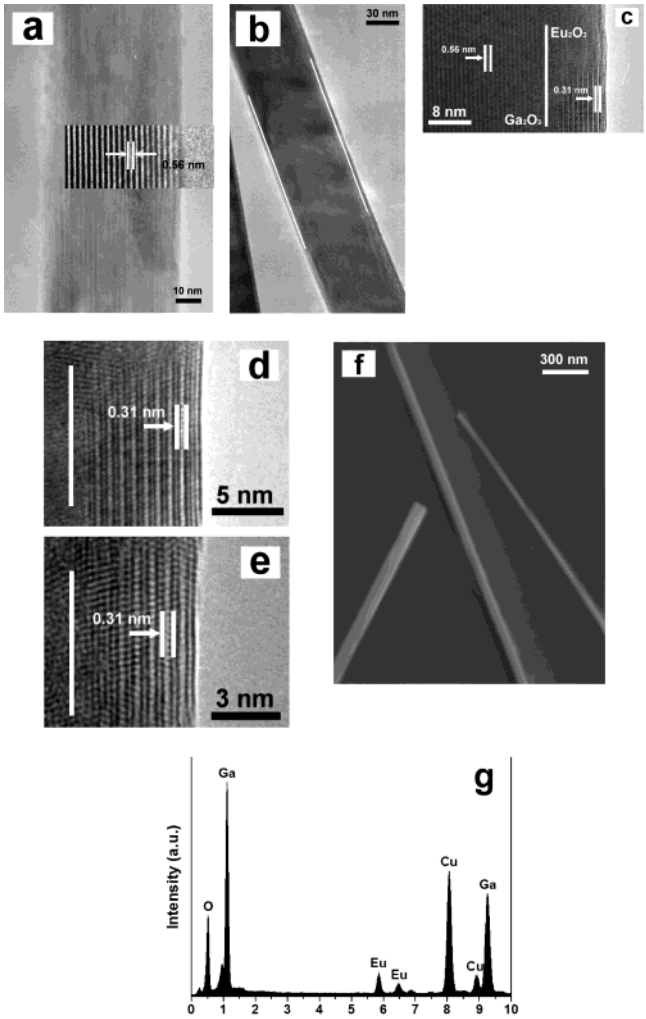

Figure 1. (a) HRTEM image of a pristine Ga_2O_3 nanoribbon. The enlarged image of the nanoribbon is shown in the inset. (b) HRTEM image of a Eu_2O_3-sheathed Ga_2O_3 nanoribbon. (c) Magnified image of the coating sheath in (b). The boundary of the europium oxide coating and Ga_2O_3 nanoribbon is indicated by a white vertical line. (d) Concentration of the europium(III) nitrate hexahydrate ethanol solution is 10 wt %. (e) Concentration of the europium(III) nitrate hexahydrate ethanol solution is 5 wt %. (f) Low-magnification SEM image of the product recorded at 15 kV without surface coating. (g) Corresponding EDX spectrum taken on a single nanoribbon reveals the presence of Ga, O, and Eu.

and the vessel was cooled to room temperature after about 24 h. CO_2 and ethanol were vented. The resulting products were ultrasonically dispersed in ethanol, filtered, and rinsed with copious amounts of ethanol to remove the uncoated europium nitrate and oxide impurities. The product was dried under vacuum.

3. Results and Discussion

3.1. Structure of the Ga_2O_3 Nanoribbons−Eu_2O_3 Multisheaths Heterostructure. Figure 1a shows a high-resolution transmission electron microscopy (HRTEM; Hitachi H-9000 operated at 300 kV) image of a pristine Ga_2O_3 nanoribbon before coating. The surfaces are clean without an amorphous layer. The lattice plane of (100) with interlayer spacing of 0.56 nm is clearly displayed. Figure 1b displays typical coated Ga_2O_3 nanoribbons found in the composite. Notably, the ribbon bodies are essentially uniformly sheathed with crystalline structures over the entire outer surface of nanoribbons. The Ga_2O_3 nanoribbons located in the middle of the europium oxide sheaths provide direct evidence for the template effect during europium oxide formation. The boundary of europium oxide coating and Ga_2O_3 nanoribbons is indicated by white parallel lines. Figure 1c depicts the magnified image of the core−sheath coaxial heterostructures shown in Figure 1b that reveals a perfect multilayered Eu_2O_3 coating on the nanoribbons and clearly displays the lattice of the sheath with an interlayer spacing of 0.31 nm, which corresponds well to an interplanar distance of the (222) planes of body centered cubic Eu_2O_3. The boundary of europium oxide coating and Ga_2O_3 nanoribbon is indicated by a white vertical line, the crystal lattices of Ga_2O_3 have not been ruined, and the Ga_2O_3 nanoribbons are still crystalline. In addition, we find that the thickness of the coating sheath could be controlled by adjusting the concentration of europium(III) nitrate hexahydrate ethanol solution. When the concentration is 10 wt %, the sheath is 7.0−8.0 nm (Figure 1d); if the concentration is halved, the sheath is 4.0−5.0 nm (Figure 1e), including about 14 concentric cylinders. A low-magnification scanning electon microscopy (SEM) image (Figure 1f) reveals that the product consists of nanoribbons in which their surfaces are uniform, without the particles of Eu_2O_3. An energy-dispersive X-ray (EDX) spectrum taken from the same sample is shown in Figure 1g, which confirms that Ga_2O_3 nanoribbons are coated by a europium oxide. Ga, O, and Eu peaks are evident in the spectrum in addition to Cu from the microscopy grid. The EDX measurement is also useful to obtain a quantitative estimate of the Eu and Eu/Ga ratio. For light elements such as oxygen, only a rough estimate could be obtained. Therefore, the Eu/O or Ga/O ratio could not be estimated from EDX spectra. From this spectrum, the ratio of Eu/Ga is estimated to be about 1:4.4.

The X-ray diffraction (XRD) patterns of the europium oxide coated Ga_2O_3 nanoribbons and pristine Ga_2O_3 nanoribbons are studied. The crystalline nature of the product is demonstrated by the presence of diffraction peaks of β-Ga_2O_3. The XRD results of the pristine Ga_2O_3 nanoribbons and Ga_2O_3 nanoribbons coated with Eu_2O_3 are the same and match the XRD (not shown here) data of β-Ga_2O_3 (JCPDS 11-370). We could not detect the XRD pattern of Eu_2O_3 because the Eu_2O_3 coating is perhaps less than the detection limit of the instrument. Shen[28] and Pol[29] reported in their study of supported europium oxides that samples containing a low concentration of europium do not appear in the XRD pattern.

X-ray photoelectron spectroscopy (XPS) is known to probe only the surface of the materials. The analysis of low-energy electrons, which are strongly scattered in materials and consequently have a small escape depth, enables information to be obtained from the top few atomic layers of a surface. The coating sheath is several nanometers, so XPS can provide us plenty of information about the interface of Ga_2O_3 and Eu_2O_3. The XPS spectra of the pristine Ga_2O_3 nanoribbons and Eu_2O_3 nanolayer coated on the nanoribbons, recorded in the energy region of the Eu(3d) transition, are presented in Figure 2. The spectrum of pristine Ga_2O_3 nanoribbons before coating shows two well-resolved peaks. The peaks are due to the Ga^{3+} ions in Ga_2O_3 assigned to Ga($2p_{3/2}$) states centered at 1119.8 eV and Ga($2p_{1/2}$) states centered at 1146.7 eV, respectively. The spectrum of nanoribbons after coating also shows two well-resolved Ga(2p) peaks. On the basis of the published Eu(3d) spectra of Eu_2O_3,[29,30] we can assign the prominent peak around 1136.7 eV to a $Eu^{3+}{}_{5/2}(3d4f^6)$ configuration. The other small peak around 1126.4 eV is attributed to a $Eu^{2+}{}_{5/2}(3d4f^7)$ configuration. The other spin−orbit component, the 3/2, appears at 1164.4 and 1157.4 eV for +3 and +2, respectively. The existence of the divalent peak is found also by others, and in fact it always accompanies the XPS of Eu^{3+} ions. The wide survey XPS spec-

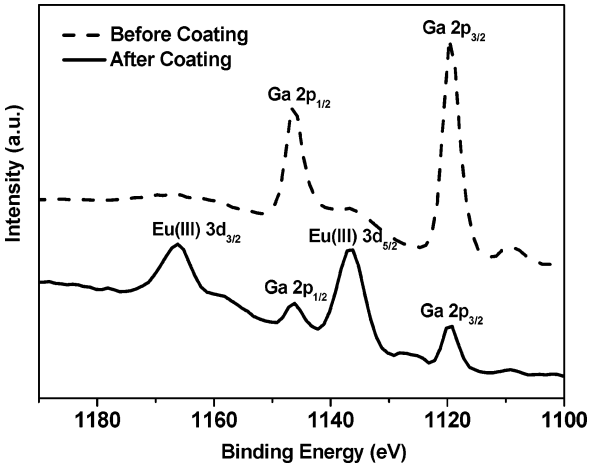

Figure 2. XPS spectra of Ga(2p) and Eu(3d) levels in the sample before coating and after coating.

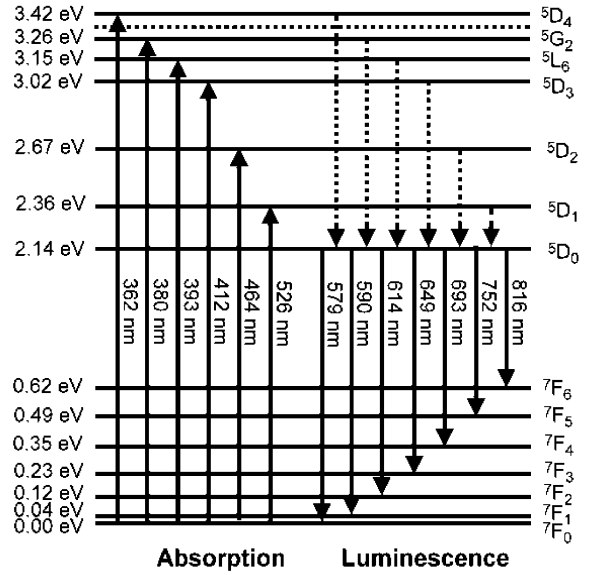

Figure 3. Energy level diagram of the optical transitions within Eu^{3+} ions.

trum of nanoribbons after coating shows the predominant presence of oxygen (78 atom %), europium (11 atom %), and gallium (11 atom %). The atomic composition reveals a prominent increase of oxygen, attributed to the oxygen atoms in the europium oxide and air absorbed on the surface of Ga_2O_3 nanoribbons. The trace content of nitrogen indicates the coating is europium oxide. It is clear from HRTEM and XPS that the coating material is Eu_2O_3 and that the gallium signal arises from the Ga_2O_3 nanoribbons. The Ga_2O_3 nanoribbons were actually sheathed within Eu_2O_3.

3.2. Optical Characterization of the Ga_2O_3 Nanoribbons−Eu_2O_3 Multisheaths Heterostructure. In our experiments, the Ga_2O_3 nanoribbons are synthesized in H_2 atmosphere at high temperature.[26] Considering the insufficiency of chemical oxidation and the inevitable defects occurring in the crystallization process, a mass quantity of oxygen vacancies would be created in the growth of Ga_2O_3 nanoribbons. These oxygen vacancies generally act as deep defect donors in semiconductors and would cause the formation of new donor levels in the band gap. In the photoexcitation process, the electron in a donor oxygen vacancy can be captured by the excited hole on an acceptor, and then a blue photon is emitted via the radiative recombination process. As a result, a striking photoluminescence (PL; Hitachi F-4500) feature showing in the Ga_2O_3 nanoribbons is that there exists a

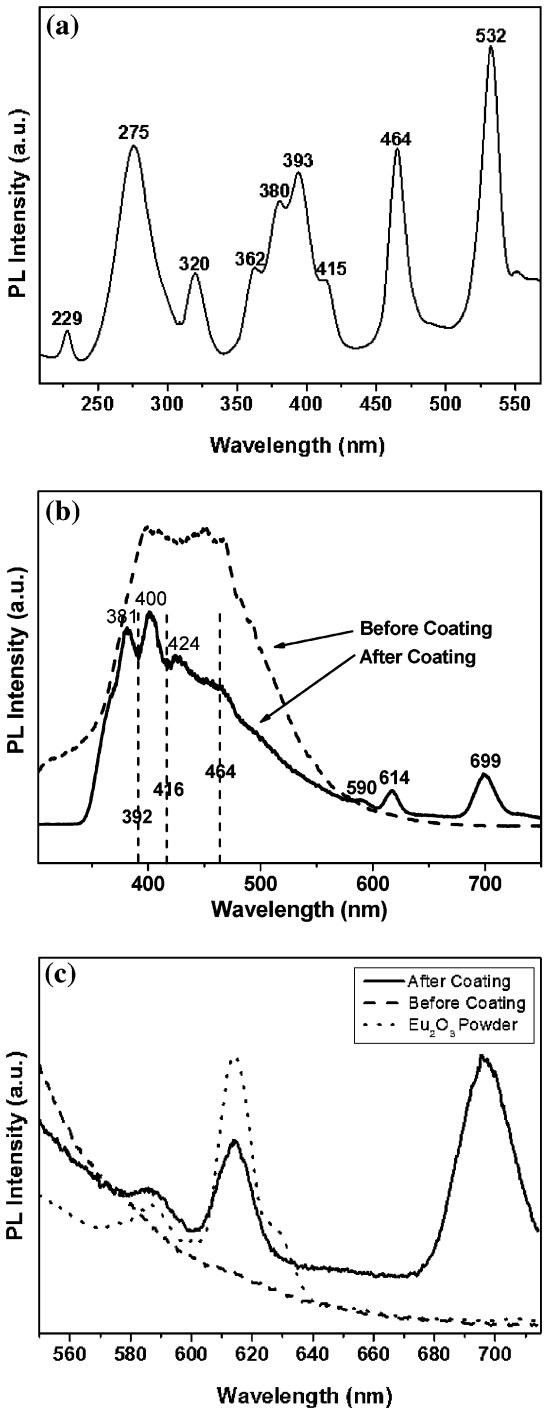

Figure 4. (a) Excitation spectrum of europium oxide; examined wavelength was 615 nm. (b) Photoluminescence spectra of Eu_2O_3-coated Ga_2O_3 nanoribbons (solid line) and pristine Ga_2O_3 nanoribbons (dashed line) at room temperature. The excitation wavelength was 250 nm and the filter wavelength was 300 nm. (c) Photoluminescence spectra of Eu_2O_3-coated Ga_2O_3 nanoribbons (solid line), pristine Ga_2O_3 nanoribbons (dashed line), and Eu_2O_3 powder (dotted line) in the red section.

strong and broad luminescence band appearing from 380 to 470 nm mainly originating from the recombination of an electron on a donor formed by oxygen vacancies. In a crystalline lattice, the transitions of Eu^{3+} are essentially free-ion-like in character.[31] These transitions are summarized in Figure 3.[32] Observed absorption and luminescence transitions are represented by a solid line; nonradiative transitions are shown as a dotted line. In summary, 362, 380, 393, 412, 464, and 526 nm photons are absorbed by the 4f → 5d transition to the charge transfer state,

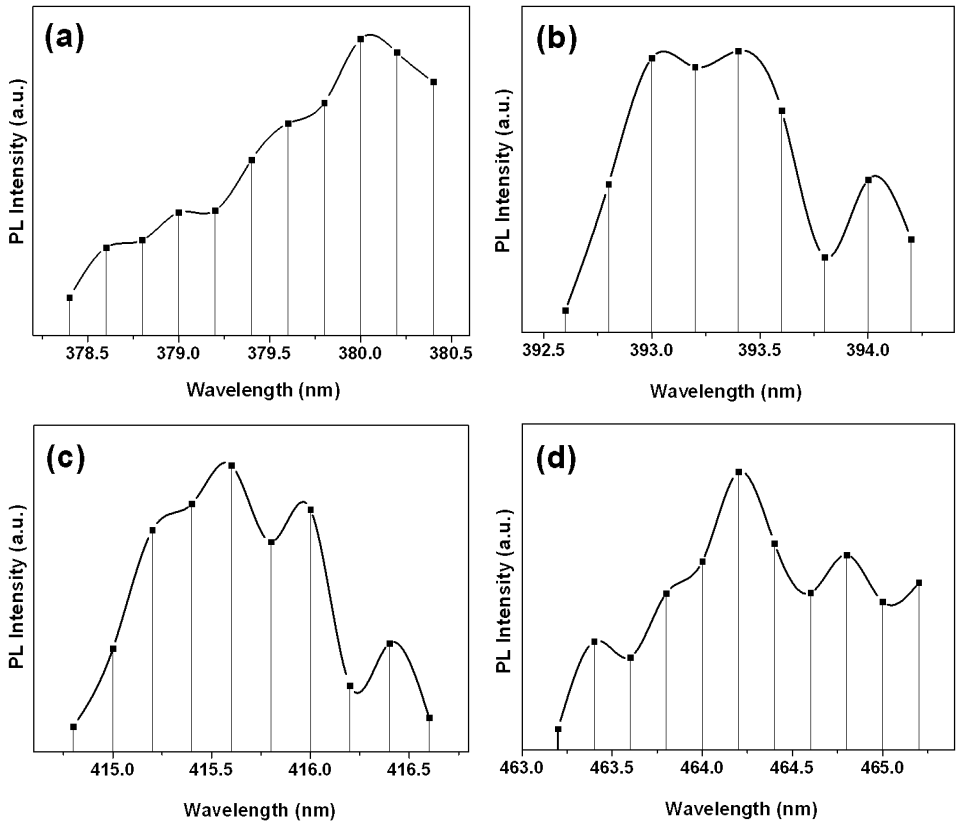

Figure 5. Absorption of Eu_2O_3 coating at (a) 380, (b) 393, (c) 416, and (d) 464 nm.

whereupon nonradiative transitions occur until the electron resides at the $^5D_0$ energy level in the 4f shell. Radiative recombination then occurs to the ^7F_J levels, with $^5D_0 \rightarrow {}^7F_2$ (614 nm) being the most intense, resulting in the Eu_2O_3 emitting in the red.

Energy transfer between a noncovalent functionalized materials and SWNTs in composite has recently been reported.[33−35] The fluorescence quenching was derived from efficient energy transfer from noncovalent functionalized materials to the nanotubes. In our experiment, the Ga_2O_3 nanoribbons are excited by the 250 nm light, and then a strong and broad luminescence band appears from 380 to 470 nm (blue light), which can be absorbed by europium oxide sheaths, resulting in the Eu_2O_3 emitting in the red (614 nm).

Photoluminescence spectra were found to give direct evidence for the interaction of the Ga_2O_3 nanoribbons and Eu_2O_3 coating. The excitation spectrum of the europium oxide nanolayer coated on Ga_2O_3 nanoribbons is shown in Figure 4a. The excitation spectrum of Eu_2O_3 in 350−600 nm is observed as several intense bands peaking at 362 ($^7F_0 \rightarrow {}^5D_4$), 380 ($^7F_0 \rightarrow {}^5G_2$), 393 ($^7F_0 \rightarrow {}^5L_6$), 415 ($^7F_0 \rightarrow {}^5D_3$), 464 ($^7F_0 \rightarrow {}^5D_2$), and 592 nm ($^7F_0 \rightarrow {}^5D_1$), respectively. These results match the published results.[34] The principal features in 210−300 nm are two bands at 229 and 275 nm, which correspond to transitions from the $^7F_0$ ground state to charge transfer states due to the europium−oxygen interaction.[36] The absorption of Eu_2O_3 nanolayers is feeble upon excitation at 250 nm. The Eu_2O_3 nanolayers mainly absorb the luminescence emission of Ga_2O_3 nanoribbons around 380−470 nm. Figure 4b shows the fluorescent spectra of europium oxide coated Ga_2O_3 nanoribbons and pristine Ga_2O_3 nanoribbons at room temperature with the same experiment conditions. We can divide the whole fluorescent spectra into two sections for better discussion: the blue section (380−470 nm) and the red section (590−720 nm). In the blue section, we were able to detect a decrease in the fluorescence intensity in the europium oxide coated Ga_2O_3 nanoribbons compared with that of the pristine Ga_2O_3 nanoribbons. It is very interesting that the flat spectrum becomes undulate after coating. Two major troughs of the spectrum after coating are 392 and 416 nm. Referring to the excitation spectrum of Eu_2O_3 (Figure 4a), we find that the two troughs correspond to two absorption peaks of Eu_2O_3: 393 ($^7F_0 \rightarrow {}^5L_6$) and 415 nm ($^7F_0 \rightarrow {}^5D_3$). This phenomenon would be derived from the efficient energy transfer from Ga_2O_3 nanoribbons to the Eu_2O_3 sheaths. The reason there are troughs at 392 and 416 nm is that the emission of Ga_2O_3 nanoribbons in this region is very strong and the curve of emission is planar. The absorptions at 380 and 464 nm are strong, and troughs located there are expected, but the curve of the emission of Ga_2O_3 nanoribbons begins to remarkably weaken from there so we cannot observe obvious troughs. We measure the absorption of Eu_2O_3 coating (the emission of Ga_2O_3 nanoribbons minus the emission of Eu_2O_3-coated Ga_2O_3 nanoribbons) about 380 (Figure 5a), 393 (Figure 5b), 416 (Figure 5c), and 464 nm (Figure 5d), and find the absorptions at those locations are obviously stronger than nearby. The emissions at 360 and 532 nm are very weak, so the absorptions are not obvious and the data are not trustworthy due to the variation of the measurement conditions or the impurity contamination. In the red section (Figure 4c), three striking emission peaks were observed at 590 ($^5D_0 \rightarrow {}^7F_1$), 614 ($^5D_0 \rightarrow {}^7F_2$), and 699 nm ($^5D_0 \rightarrow {}^7F_4$) in the europium oxide coated Ga_2O_3 nanoribbons, but were absent in the pristine Ga_2O_3 nanoribbons. There are two emission peaks at 590 and 610 nm in the fluorescence spectrum of Eu_2O_3 powder (measured upon excitation at 250 nm), which are due to Eu_2O_3 excited to a higher excited state, and via radiationless transition reaches the $^5D_0$ emitting state. It is interesting to note that the most intense emission of europium oxide coated Ga_2O_3 nanoribbons arises from the $^5D_0 \rightarrow {}^7F_4$ transition (forced electric

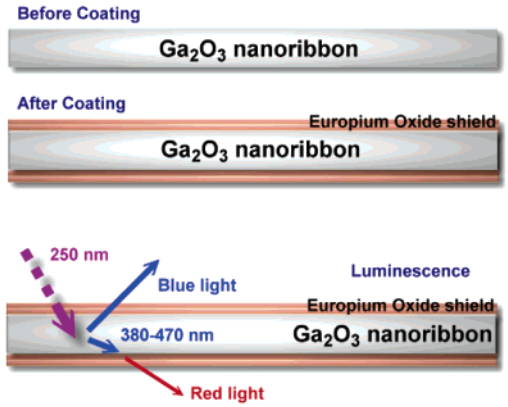

Figure 6. Schematic presentation of the formation of $Ga_2O_3-Eu_2O_3$ core−sheath coaxial nanoribbons and luminescence mechanism. The Ga_2O_3 nanoribbons are excited by 250 nm light; then a strong and broad luminescence band appears from 380 to 470 nm (blue light), which can be absorbed by europium oxide sheaths, resulting in Eu_2O_3 emitting in the red.

dipole transition). The $^5D_0 \rightarrow {}^7F_2$ transition (electric quadrupole transition), which is predominant in Eu_2O_3 powder, has a low intensity and is the second most intense emission of the spectra. Possibly it involves the energy transfer from Ga_2O_3 nanoribbon emission to Eu_2O_3 coating on the nanoribbons, which enriches its intensity. This causes a charge transfer reaction with the Eu^{3+} metal cations during the 4f−4f electronic transitions. The effect seems to be pronounced in the $^5D_0 \rightarrow {}^7F_2$ transition. Such a phenomenon was first observed in our study and has not yet been reported. This needs further study to reach an acceptable model of its excitation to account for the enormously large photoemission intensity. The formation of $Ga_2O_3-Eu_2O_3$ core−sheath coaxial nanoribbons and luminescence mechanism can then be clarified as is schematically illustrated in Figure 6.

4. Conclusion

In this paper, by using a simple low-temperature supercritical fluid assisted method, Ga_2O_3 nanoribbons coated with crystalline multilayer europium oxide sheaths have been successfully synthesized, with a nominally uniform coating over the entire outer surface of the nanoribbons. It shows novel energy transfer between the core and the sheath at room temperature. The methodology reported here is highly versatile, and we focus on the $Ga_2O_3-Eu_2O_3$ core−sheath coaxial nanoribbons only as a showcase introduction to this powerful synthetic approach. It should be possible to fabricate highly crystalline core−sheath heterostructures of many other complex materials using different nanoribbons or nanowires (GaN, ZnO, Si) as substrates or introducing appropriate precursors (other rare-earth elements or transition-metal elements) as coating sheaths into the reaction chamber. Important features of this one-dimensional nanostructure based approach to coaxial heterostructure formation reside in its flexibility in materials choice, synthetic simplicity, low temperature, and chemical solution, which differ significantly from previously reported.[37−40] The high chemical reactivity of nanoribbons and nanowires due to their low dimensionality and high surface-to-volume ratio leads them to be easily oxidized and contaminated, resulting in dramatic changes in structure and properties. Our method can be used to coat a protective sheath made of thermally and chemically stable materials on a given nanowire to enhance its performance, which is particularly important for the fabrication of nanodevices. These core−sheath heterostructures represent a novel class of highly functional, one-dimensional nanoscale building blocks for nanoribbons or nanowire-based devices.

Acknowledgment. The authors gratefully acknowledge financial support from the National Natural Science Foundation of China (NNSFC), the Major State Basic Research Development Program, and the Chinese Academy of Sciences.

References and Notes

(1) Sze, S. M. *Physics of Semiconductor Devices*; Wiley-Interscience: New York, 1981.
(2) Hu, J. T.; Ouyang, M.; Yang, P. D.; Lieber, C. M. *Nature* **1999**, *399*, 48.
(3) Cui, Y.; Lieber, C. M. *Science* **2001**, *291*, 851.
(4) Duan, X. F.; Huang, Y.; Cui, Y.; Wang, J. E.; Lieber, C. M. *Nature* **2001**, *409*, 66.
(5) Huang, Y.; Duan, X. F.; Cui, Y.; Lauhon, L. J.; Kim, K. H.; Lieber, C. M. *Science* **2001**, *294*, 1313.
(6) He, R.; Law, M.; Fan, R.; Kim, F.; Yang, P. *Nano Lett.* **2002**, *2*, 1109.
(7) Hu, J.; Bando, Y.; Liu, Z.; Sekiguchi, T.; Golberg, D.; Zhan, J. *J. Am. Chem. Soc.* **2003**, *125*, 11306.
(8) Gudiksen, M. S.; Lauhon, L. J.; Wang, J.; Smith, D. C.; Lieber, C. M. *Nature* **2002**, *415*, 617.
(9) Bjork, B. T.; Ohlsson, B. J.; Sass, T.; Persson, A. I.; Thelander, C.; Magnusson, M. H.; Deppert, K.; Wallenberg, L. R.; Samuelson, L. *Appl. Phys. Lett.* **2002**, *80*, 1058.
(10) Bjork, M. T.; Ohlsson, B. J.; Sass, T.; Persson, A. I.; Thelander, C.; Magnusson, K.; Deppert, M. H.; Wallenberg, L.; Samuelson, R. L. *Nano Lett.* **2002**, *2*, 87.
(11) Wu, Y.; Fan, R.; Yang, P. *Nano Lett.* **2002**, *2*, 83.
(12) Lauhon, L. J.; Gudiksen, M. S.; Wang, D. L.; Lieber, C. M. *Nature* **2002**, *420*, 57.
(13) Reisfeld, R.; Yorgensen, C. K. *Lasers and Excited States of Rare Earth*; Springer-Verlag: New York, 1977.
(14) Sheng, K. C.; Korenowski, G. M. *J. Phys. Chem.* **1988**, *92*, 50.
(15) Tissue, B. M. *Chem. Mater.* **1998**, *10*, 2837.
(16) Patra, A.; Sominska, E.; Ramesh, S.; Koltypin, Y.; Zhong, Z.; Minti, H.; Reisfeld, R.; Gedanken, A. *J. Phys. Chem. B* **1999**, *103*, 3361.
(17) Choi, Y. C.; Kim, W. S.; Park, Y. S.; Lee, S. M.; Bae, D. J.; Lee, Y. H.; Park, G.; Choi, W. B.; Lee, N. S.; Kim, J. M. *Adv. Mater.* **2000**, *12*, 746.
(18) Liang, C. H.; Meng, G. W.; Wang, G. Z.; Wang, Y. W.; Zhang, L. D. *Appl. Phys. Lett.* **2001**, *78*, 3202.
(19) Dai, Z. R.; Pan, Z. W.; Wang, Z. L. *J. Phys. Chem. B* **2002**, *106*, 902.
(20) Sharma, S.; Sunkara, M. *J. Am. Chem. Soc.* **2002**, *124*, 12288.
(21) Hu, J. Q.; Bando, Y.; Liu, Z. W. *Adv. Mater.* **2003**, *15*, 1000.
(22) Ma, R. Z.; Bando, Y. *Chem. Phys. Lett.* **2003**, *367*, 219.
(23) Edwards, D. D.; Mason, T. O.; Goutenoir, F.; Poeppelmeimer, K. R. *Appl. Phys. Lett.* **1997**, *70*, 1706.
(24) Ogita, M.; Saika, N.; Nakanishi, Y.; Hatanaka, Y. *Appl. Surf. Sci.* **1999**, *142*, 188.
(25) Weh, T.; Frank, J.; Fleischer, M.; Meixner, H. *Sens. Actuators, B* **2001**, *78*, 202.
(26) Fu, L.; Liu, Y.; Hu, P.; Xiao, K.; Yu, G.; Zhu, D. *Chem. Mater.* **2003**, *15*, 4287.
(27) Eckert, C. A.; Knutson, B. L.; Debenedetti, P. G. *Nature* **1996**, *383*, 313.
(28) Shen, J.; Lochhead, M. J.; Bray, K. L.; Chen, Yi.; Dumesic, J. A. *J. Phys. Chem.* **1995**, *99*, 2384.
(29) Pol, V. G.; Reisfeld, R.; Gedanken, A. *Chem. Mater.* **2002**, *14*, 3920.
(30) Cho, E. J.; Oh, S. J.; Suga, S.; Suzuki, T.; Kasuya, T. *J. Electron Spectrosc. Relat. Phenom.* **1996**, *77*, 173.
(31) Dieke, G. H. *Spectra and Energy Levels of Rare Earth Ions in Crystals*; Interscience: New York, 1968.
(32) Carnell, W. T.; Field, P. R.; Rajnak, K. *J. Chem. Phys.* **1968**, *49*, 4450.
(33) Tang, B. Z.; Xu, H. Y. *Macromolecules* **1999**, *32*, 2569.
(34) Chen, J.; Liu, H.; Weimer, W. A.; Halls, M. D.; Waldeck, D. H.; Walker, G. C. *J. Am. Chem. Soc.* **2002**, *124*, 9034.
(35) Murakami, H.; Nomura, T.; Nakashima, N. *Chem. Phys. Lett.* **2003**, *378*, 481.
(36) Yin, M.; Zhang, W.; Xia, S.; Krupa, J.-C. *J. Lumin.* **1996**, *68*, 335.
(37) Shi, W. S.; Peng, H. Y.; Xu, L.; Wang, N.; Tang, Y. H.; Lee, S. T. *Adv. Mater.* **2000**, *12*, 1927.
(38) Meng, X. M.; Hu, J. Q.; Jiang, Y.; Lee, C. S.; Lee, S. T. *Appl. Phys. Lett.* **2003**, *83*, 2241.
(39) Kim, H. Y.; Bae, S. Y.; Kim, N. S.; Park, J. *Chem. Commun.* **2003**, 2634.
(40) Li, Q.; Wang, C. *J. Am. Chem. Soc.* **2003**, *125*, 9892.